AUT Journal of Mechanical Engineering

AUT J. Mech. Eng., 5(4) (2021) 497-510
DOI: 10.22060/ajme.2021.19099.5932

Suspension Design Optimization of a Hermetic Compressor for Improved Vibrational Behavior

A. Kogani, F. A. Shirazi*, M. J. Mahjoob

Department of Mechanical Engineering, University of Tehran, Tehran, Iran

ABSTRACT: Abnormalities in the vibrational behavior of driving motors and their side effects have always been a chief concern for home appliance manufacturers. Hermetic compressors used in refrigerators are no exception in this matter. As a single-piston reciprocating machine with a crankshaft driven by a simple rotor-stator system, compressors can have noticeable vibrational dissonances. The compressor's vibration is considered as a source of noise that can be transferred to other parts of the refrigerator and disturbingly excite them. Despite multiple studies to isolate this vibration by removing or optimizing its pathways, the focus has never been directly on reducing the vibration of the main source. In this study, a 6 Degree of Freedom model of a refrigerator compressor is derived and then simulated in MATLAB-Simulink. The model is then verified with the computational results of an equivalent model made in ADAMS. All vibrating parts and their indexes are identified in order to design a new suspension system with improved vibrational behavior. A genetic algorithm is used to minimize an acceleration-based objective function considering six optimization variables including the stiffness parameters of springs and their arrangement. The optimized springs were built and tested under an actual compressor, and the time/frequency responses of the compressor were compared with the initial system. The results show the enhanced vibrational behavior of the compressor in its working frequency after optimization.

Review History:

Received: Oct. 06, 2020
Revised: Jan, 06, 2021
Accepted: Jan, 22, 2021
Available Online: Jan, 30, 2021

Keywords:

Refrigerator hermetic compressor
Vibration
Suspension system
Genetic algorithm
Optimization

1- Introduction

Hermetic compressors are the main components of many refrigerating systems. These compressors have a compact form that offers a compatible, portable option for refrigerator manufacturers. Mechanically, compressors can be considered as two-part devices. The internal part consists of the rotor, stator, crankshaft, piston, and other components of the compression process, and the hard outer shell that protects the inner parts and seals everything within, including the whole compressing assembly, refrigerant gas, and lubricant oil. These two components are connected by a suspension system consisting of three or four springs and a discharge pipe that takes the compressed refrigerant out. The connecting parts contribute to the transmitted vibration generated by the rotating crankshaft [1], and therefore they need to be properly designed to prevent vibration problems.

Generally, vibration control can be achieved by three methods of isolation from the source, in the path, and at the receiver [2]. Refrigerator compressors can be considered in the same way, where all three approaches are applicable. However, most of the efforts have been made to keep the vibration isolated from other parts of the refrigerator using the second approach, i.e. controlling in the path. The inlet and outlet pipes of the refrigerant gas connect the inside core and the rigid outer shell. This connection may act as a vibration transmitter that disturbingly excites other parts of the refrigerator. Suk et al. [3] investigated these pipelines and designed the pipes in an innovative approach to reduce the vibration transmission.

From the engineering point of view, vibration isolators are systems that react to the vibration and dynamic excitation of an object to mitigate the undesirable effects of its transmission [4]. Brungart and Riggs [5] used a single layer of an elastomer in a marine propulsor to reduce its vibration (isolation mount). The rotating feature of the propulsors and their interaction with non-uniform flow generated unwanted vibrations that needed to be examined. The modified rotor showed a reduction of 15 dB in transmissibility compared to the rotor with no isolation. Jihuyn Lee et al. [6], investigated the location of passive vibration isolators to minimize the unwanted exogenous vibrations. By assuming known stiffness and damping coefficients of the isolators, they focused on optimizing their locations. They managed to reduce the (vibration) cost function by reformulating the nonlinear problem as a Linear Time-Invariant (LTI) one and using methods of optimal control theory. The framework turned out to be applicable to passive isolators/dampers in automotive, aerospace, and other applications. Gardonio and Elliott [7], tried to reduce the transmitted vibration between two plates,

*Corresponding author's email: fshirazi@ut.ac.ir

connected by a mounting system using an impedance-mobility matrix. The effects of different active and passive isolators were investigated with simulation. Furthermore, they choose the proper isolator material for a specific vibration system by defining an optimization problem. Gou et al. [8] investigated the effects of nonlinear viscous dampers on absorbing the force/energy applied on an isolator system. An analytical algorithm was obtained via Ritz-Galerkin method to study the force transmission in a vibrating system that uses damping rubbers to absorb energy. The results showed that the nonlinear rubber dampers were more efficient than their linear counterparts in a wide frequency range.

The suspension system optimization problem is more of a standard design issue in vehicles than refrigerator compressors. Auto-manufacturers have to design and modify the car suspension systems, depending on the operating conditions. Zehsaz et al. [9] investigated a tractor suspension system and optimized its vibrational behavior. They calculated the FRFs and measured vibration indexes using accelerometers connected to the cabin in road conditions at different speeds. Modeling of the vibration system in a finite element software was also conducted simultaneously. Optimization was then performed to determine the optimal values of the system parameters. They observed a significant dynamic improvement comparing the final and initial results. Zhongzhe chi et al. [10] compared three optimization methods: Genetic Algorithm (GA), Porcellio Scaber Algorithm (PSA), and Sequential Quadratic Programming (SQP) for a vehicle suspension system to minimize passenger's cabin acceleration. SQP was more successful in finding local minima, while the other two were more compatible in finding global optimal points. The total acceleration of springs was reduced by 32.8% after optimizing the vehicle suspension system. Mahmudi et al. [11] studied the optimization of suspension system in an off-road vehicle. The vehicle suspension system and road conditions were modeled in ADAMS. Then, GA optimization was used to achieve a better cabin comfort, stability, and handling of the vehicle. The results were compared with a baseline model in ADAMS and experimental data. Reddy et al. [12] investigated a vehicle suspension system for improving cabin comfort with GA and RSM methods. Results showed the effectiveness of both approaches in finding optimal points for stiffness and damping coefficients.

A survey of the literature shows that the studies related to suspension system optimization have mainly focused on vehicles. Also, the works that have focused on the refrigerator compressor's vibrations were not aiming at the primary source. The approach adopted in this paper has therefore not been attempted in the previous works mentioned in the literature.

Here, a hermetic compressor modeled in Computer-Aided Design (CAD) environment including all parts is brought into ADAMS for vibration analysis. Boundary conditions are then applied, and suspension springs are assembled in the model. The exciting external forces in the system are included and studied in the ADAMS model. The compressor is also modeled as a 6-Degree of Freedom (DoF) system in Simulink for design and optimization process. ADAMS and Simulink models are compared for verification under similar applied forces and boundary conditions. After completing the model and ensuring its accuracy, the optimization is carried out. The suspension system of the compressor is optimized with respect to the stiffness of its main springs and their arrangement under the compressor. The final suspension is tested in a real compressor system and the experimental results are demonstrated.

2- Simulation and Optimization

2- 1- System description

The compressor used in this study is a ½ hp Zanussi hermetic compressor (by PADENA Compressor manufacturers). The compressor and its CAD models are shown in Fig. 1. The interior structure of the compressor is composed of the main block for the compression chamber, valves and pathways for refrigerant, the stator block and windings, rotor, crankshaft and piston, and the suspension system including springs and damping rubbers. In each cycle of compression, the refrigerant is sucked from the condenser and pushed into the evaporator in the refrigerator.

2- 2- Dynamic model

The compressor is dynamically modeled as a 6-DoF rigid body, supported by four compression springs. A coordinate system with the origin located at the compressor's Center of Gravity (CG) is considered. It is assumed that *Z*-axis is parallel to the crankshaft axis, as shown in Fig. 2. The 6-DoF model of the compressor is described as follows.

The central part has 6 DoFs, three displacements, *X, Y, Z* and three rotations φ, θ and ψ along the three main axes. The four points connecting the main springs to the compressor have been indexed by 1 to 4 numerically. The distance of the CG from all four spring contact points has been shown and named accordingly. The distance of the CG along the *Z*-axis from all four positions is equal (*d*). Along About *Y*-axis, the compressor is symmetric and is divided into two equal parts (*L*), and finally, in the *X*-axis direction, the compressor model is divided into two unequal portions (*a* and *b*). The main springs are indicated with a single stiffness coefficient (*K*). A schematic view of the suspension system at contact point 1 is shown in Fig. 2. The other three have the same arrangement as point 1. The main springs have considerable lateral stiffness (*k'*) that should be considered in the system's dynamic equations. For a steel spring, the lateral stiffness can be calculated from [13]

$$\frac{K}{k'} = 1.44C_1\left[0.204\left(\frac{h_S}{D}\right)^2 + 0.265\right] \quad (1)$$

Where *K* is the vertical stiffness, *D* is the spring diameter, *k'* is lateral stiffness, h_s is spring length under vertical load, and C_1 is a coefficient determined by aspect ratio and vertical deflection.

Fig. 1. Hermetic compressor and its CAD model

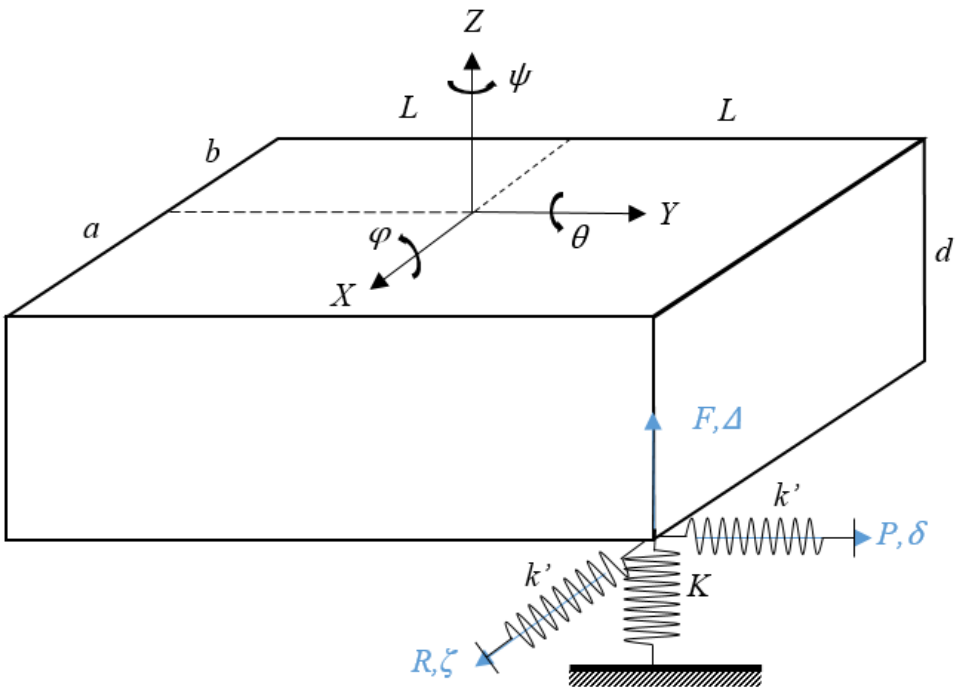

Fig. 2. 6-DOF model of compressor

Any displacement of the four corners in any direction will cause tension in springs; therefore, forces will apply to the main body from these contact points. Forces and displacements in the three main directions are shown in Fig. 2 at a typical corner. They are also listed in Table 1. Each corner has its own subscript number for forces and displacements in the equations. In order to obtain the dynamic equations of motion the Lagrange's method was employed as follows:

Kinetic Energy:

$$T = \frac{1}{2}M(\dot{Z}^2 + \dot{X}^2 + \dot{Y}^2) + \frac{1}{2}I_\varphi\dot{\varphi}^2 + \frac{1}{2}I_\theta\dot{\theta}^2 + \frac{1}{2}I_\psi\dot{\psi}^2 \quad (2)$$

Potential Energy:

$$V = \frac{K}{2}(\Delta_1^2 + \Delta_2^2 + \Delta_3^2 + \Delta_4^2) + \frac{k'}{2}(\delta_1^2 + \delta_2^2 + \delta_3^2 + \delta_4^2) + \frac{k'}{2}(\zeta_1^2 + \zeta_2^2 + \zeta_3^2 + \zeta_4^2) \quad (3)$$

Lagrangian:

$$\frac{d}{dt}\left(\frac{\partial L}{\partial \dot{q}_j}\right) - \frac{\partial L}{\partial q_j} = F_j \quad (4)$$

where $L = T - V$

For further analysis in this paper, forces will be added to this equation. The equations for free vibration are obtained as follows:

$$M\ddot{X} + R_1 + R_2 + R_3 + R_4 = F_x \quad (5)$$

$$M\ddot{Y} + P_1 + P_2 + P_3 + P_4 = F_y \quad (6)$$

$$M\ddot{Z} + F_1 + F_2 + F_3 + F_4 = F_z \quad (7)$$

$$I_\varphi\ddot{\varphi} + \overline{dL}\cos\gamma_{21}(F_1 + F_2) + \overline{dL}\cos\gamma_{23}(F_3 + F_4) - \overline{dL}\sin\gamma_{21}(P_1 + P_2) - \overline{dL}\sin\gamma_{23}(P_3 + P_4) - (I_\theta - I_\varphi)\dot{\theta}\dot{\psi} = M_\varphi \quad (8)$$

$$I_\theta\ddot{\theta} + \overline{ad}\cos\beta_{21}(F_1 + F_3) + \overline{bd}\cos\beta_{22}(F_2 + F_4) + \overline{ad}\sin\beta_{21}(R_1 + R_3) + \overline{bd}\sin\beta_{22}(R_2 + R_4) - (I_\psi - I_\varphi)\dot{\varphi}\dot{\psi} = M_\theta \quad (9)$$

$$I_\psi\ddot{\psi} - \overline{aL}\sin\Omega_{21}(P_1) - \overline{bL}\sin\Omega_{22}(P_2) - \overline{aL}\cos\Omega_{23}(P_3) - \overline{bL}\sin\Omega_{24}(P_4) - \overline{aL}\cos\Omega_{21}(R_1) - \overline{bL}\cos\Omega_{22}(R_2) - \overline{aL}\cos\Omega_{23}(R_3) - \overline{bL}\cos\Omega_{24}(R_4) - (I_\varphi - I_\theta)\dot{\varphi}\dot{\theta} = M_\psi \quad (10)$$

where,

$$\beta_{11} = \pi + \arctan(d/a)$$
$$\beta_{12} = 3\pi/2 + \arctan(b/d)$$
$$\beta_{21} = \beta_{11} + \theta$$
$$\beta_{22} = \beta_{12} + \theta$$

$$\gamma_{11} = 3\pi/2 + \arctan(L/d)$$
$$\gamma_{13} = \pi + \arctan(d/L)$$
$$\gamma_{21} = \gamma_{11} + \varphi$$
$$\gamma_{23} = \gamma_{13} + \varphi$$

$$\Omega_{11} = 3\pi/2 + \arctan(L/a)$$
$$\Omega_{12} = \arctan(b/L)$$
$$\Omega_{13} = \pi + \arctan(a/L)$$
$$\Omega_{14} = \pi/2 + \arctan(L/b)$$

Table 1. Forces and proportional displacements at the corners

Direction	***X***	***Y***	***Z***
Force	*R*	*P*	*F*
Displacement	ζ	δ	Δ
Relation between displacement and force	$k'\zeta$	$k'\delta$	$K\Delta$

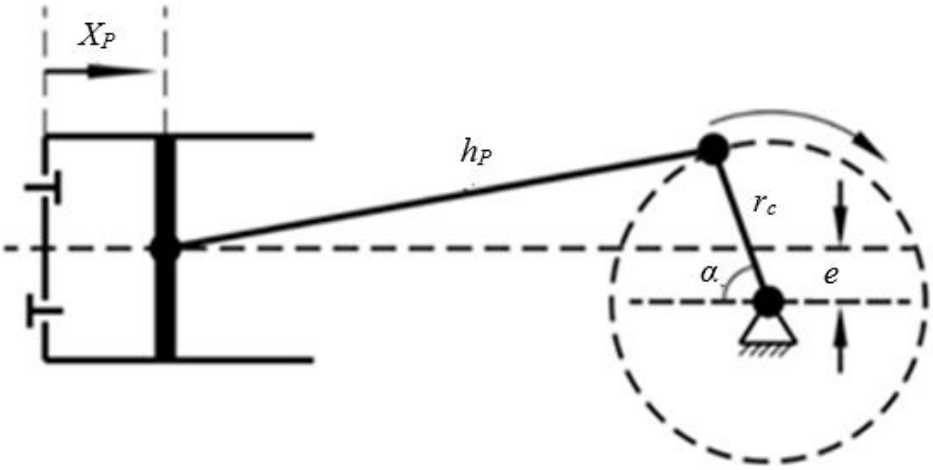

Fig. 2. Schematic of the piston-cylinder-crankshaft with related variables/parameters

$$\Omega_{21} = \Omega_{11} + \psi$$
$$\Omega_{22} = \Omega_{12} + \psi$$
$$\Omega_{23} = \Omega_{13} + \psi$$
$$\Omega_{24} = \Omega_{14} + \psi$$

$$\overline{ad} = \sqrt{a^2 + d^2}$$
$$\overline{bd} = \sqrt{b^2 + d^2}$$
$$\overline{dL} = \sqrt{d^2 + L^2}$$

This 6-DoF system has been simulated and analyzed/ solved in MATLAB-Simulink. The remaining parts of the model, such as forces will be discussed in the next section. Optimization will also take place in an iterative manner between Simulink and MATLAB.

2- 3- Forces

The force exerted on the system consists of two main components. Both of these force components are applied in a plane parallel to the *XY* plane and at the height of 51 mm from CG, aligned with the piston/cylinder. The reciprocating motion of the piston causes a sinusoidal force in the cylinder direction *(X);* the other force is caused by an unbalanced mass on top of the crankshaft produced by the crankshaft's rotation and is applied on the *XY* plane.

2- 3- 1- Piston force

The cyclic motion of the piston in the cylinder is shown in Fig. 3. It depends on the crankshaft's rotational speed and can be evaluated by the following equation [14].

$$x_p = r_c[(1 - Cos\,\alpha) + \frac{\lambda}{4}(1 - \cos 2\alpha) - e\lambda Sin\alpha] \quad (11)$$

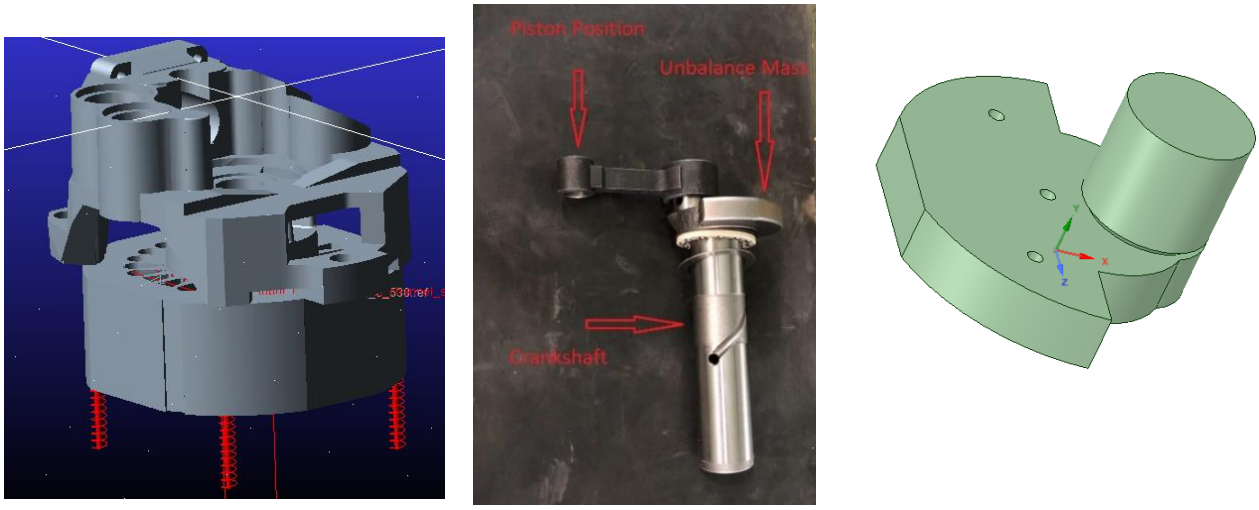

(a) (b) (c)

Fig. 4. (a) 3D model of Compressor in ADAMS (b) Crankshaft (c) Unbalanced top mass of the crankshaft

in which,

$$e = 0$$

$$\lambda = \frac{r_c}{h_p}$$

Acceleration can then be obtained thru the second derivative of the displacement as follows:

$$a_P = r_c[(1+\omega^2 \operatorname{Cos}(\omega t) + \frac{\lambda}{4}(1+4\omega^2 \operatorname{Cos}(2\omega t))]$$

$$F_{px} = m_p a_p \tag{12}$$

$$F_{py} = 0$$

Where α is rotational acceleration, ω is rotational speed, and m_p is the piston's mass.

2- 3- 2- Unbalanced mass

The forces generated due to the unbalanced masses are [15]:

$$F_{ux} = m_u \varepsilon \omega^2 Sin(\omega t) \tag{13}$$

$$F_{uy} = m_u \varepsilon \omega^2 Cos(\omega t) \tag{14}$$

Where m_u is the unbalanced mass on top of the crankshaft and ε is the distance between the rotational axis and the unbalanced mass center of gravity. Both of these parameters have been measured using a CAD model driven from the in-hand part shown in Fig. 4 (b) and (c).

In the *X*-direction, the piston force and unbalanced force are in opposite directions and must be subtracted in all periods long.

$$F_x = F_{px} - F_{ux}$$
$$F_y = F_{uy} \tag{15}$$

Each one of these forces will produce a moment about the CG proportional to its direction, magnitude, and distance from the CG (l_z).

$$F_\theta = l_z F_x$$
$$F_\varphi = l_z F_y \tag{16}$$

F_X , F_Y , F_φ , and F_θ will be applied in Eqs. (5) to (6) and (8) to (9).

2- 4- ADAMS model

The compressor was modeled as a rigid steel body with a density of 7801 kg/m^3 in ADAMS, as shown in Fig. 4(a) to compare with the dynamic model of the system derived in section 3.

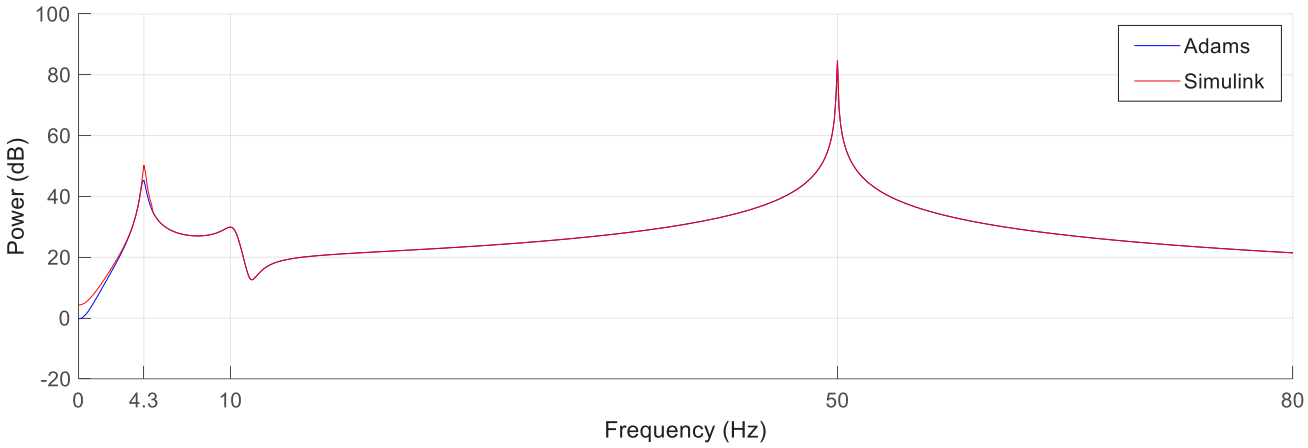

(a)

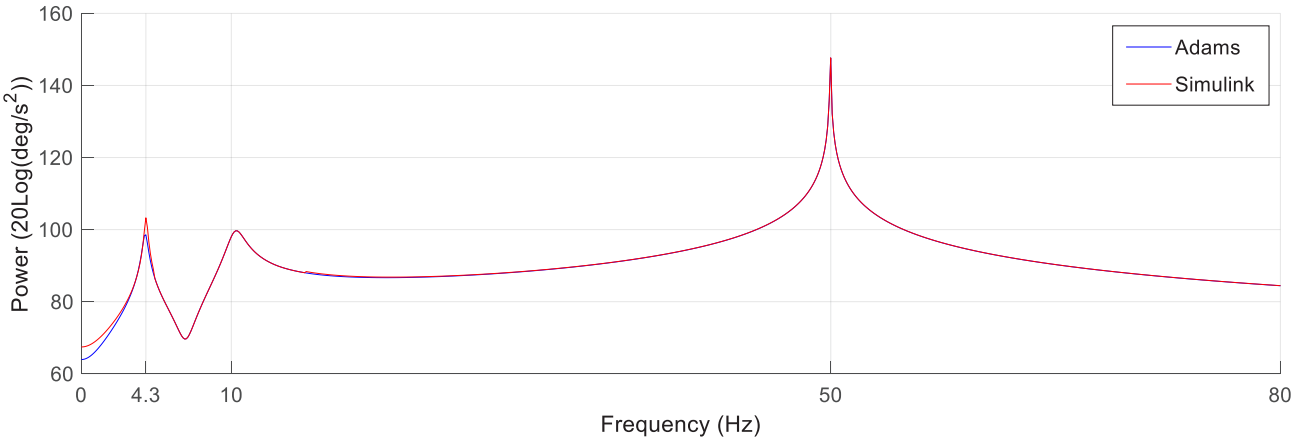

(b)

Fig. 5. Center of gravity PS acceleration comparison in MATLAB and ADAMS (a) in the X direction (b) in the θ direction

For verification purposes, a particular analysis was done using Simulink and ADAMS models, and the outputs were compared in the frequency domain. A sinusoidal force with a frequency of 50 Hz and a random amplitude of 20 N was applied in the *X* direction for both models. Simultaneously, a similar force but with a phase difference of π/2 was applied in the *Y* direction. Both forces were applied to the actual force point. The acceleration response of CG was computed for both models. Each data set were then passed to MATLAB for frequency analysis. The Power Spectrum (PS) for both transfer (*X*) and rotation (*θ*) parameters were calculated from time vs. acceleration. The Power spectrums in both variables are shown in Fig. 5. The numerical values of the peak frequencies for both methods and their percentage errors are listed in Table 2. The numerical values of all parameters used in Eqs. (1) and (5) to (10) are listed in Table 3. These values were determined based on the CAD model and information given by the compressor manufacturer.

The differences between the first peak frequency associated with the lumped approach in deriving the dynamic model of the compressor. However, as seen in Fig. 5, there is an acceptable agreement between the responses and the dynamic lumped model which will be used in the next section for the optimization.

2- 5- Optimization problem

The purpose of optimization is to reduce the vibrations of the system at the working frequency (50 Hz) by designing an optimal suspension system. The compressor crankshaft rotates at a constant speed causing a harmonic excitation

Table 2. Peak frequencies of acceleration in two X and θ directions

	First Peak Frequency (Hz)	Second Peak Frequency (Hz)	Third Peak Frequency (Hz)
ADAMS	4.295	10	50
Simulink	4.301	10	50
Error %	0.1	0	0

Table 3. Initial physical parameters of the compressor model

Parameter	K(N/m)	L(mm)	a(mm)	b(mm)	M(kg)	I_φ(kg.mm^2)	I_θ(kg.mm^2)	I_ψ(kg.mm^2)	C_1	D(mm)	h_s
Magnitude	4838	41.25	41.25	41.25	5.49	126.6	116.5	96.69	1.25	12.2	33

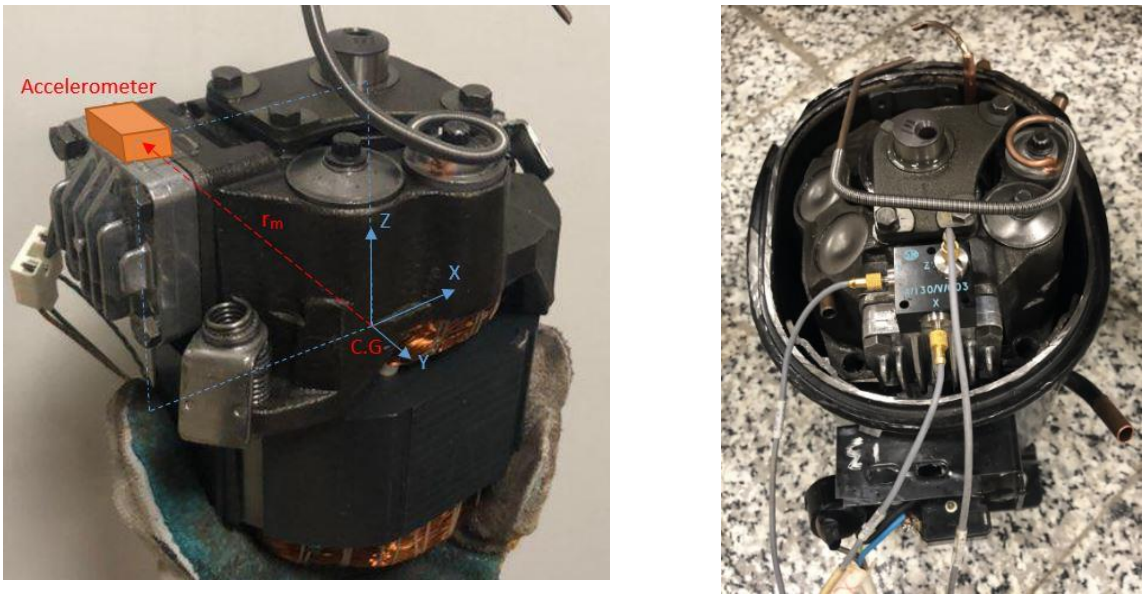

Fig. 6. Position of the accelerometer with respect to CG

in the system. Knowing the amplitude and direction of the exciting force, the compressor geometry, and mass properties, optimization of the suspension system can be formulated.

2- 5- 1- Objective function

The vibrations of the compressor must be evaluated in a specified time period that comprises a complete cycle of motion. Here, the main purpose is to reduce the vibrations of the compressor during its working conditions. Therefore, the optimization objective must be a function consisting of all motions in that period. Furthermore, the location where the acceleration is being examined must be accessible for experimental measurements (Fig. 6). Accelerations in all three directions were considered as in Eq. (17).

$$ObjectiveFunction = \sqrt{[RMS(a_m.\bar{i})]^2+[RMS(a_m.\bar{j})]^2+[RMS(a_m.\bar{k})]^2} \quad (17)$$

$$RMS(X)=\sqrt{\frac{1}{n}\left(x_1^2+x_2^2+\ldots+x_n^2\right)} \quad (18)$$

where, (i, j, k) are the unit vectors of (X, Y, Z) and n is the sample size.

Table 4. Lower and upper bounds of optimization parameters

Parameters	Lower Bound	Upper Bound
Spring Wire Diameter d (mm)	0.8	2
Spring Coil Diameter D (mm)	8	20
Coil Number N_a	3	15
Closing Index ζ	0.15	20

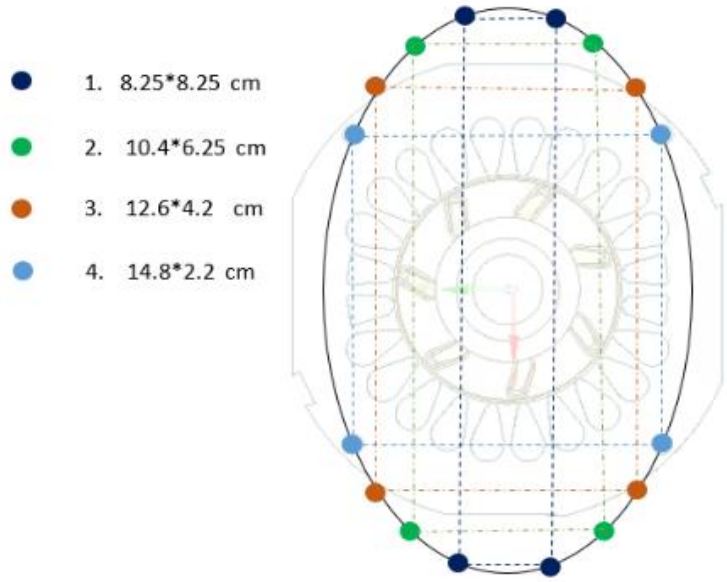

Fig. 7. Eligible arrangements for compression springs under the compressor

2- 5- 2- Optimization parameters

The stiffness of the four main springs (K) is the main parameter which, itself, contains five distinct and changeable spring design variables. Any change in main springs' stiffness will change their lateral stiffness as well and will cause a whole different dynamic behavior of the system. The optimization parameters and their chosen constraints are shown in Table 4 [16].

The fifth optimization parameter refers to the material forming the spring's wire chosen from: Music wire, Hard-Drawn wire, Chrome-Vanadium, and Chrome-Silicon.

The sixth and final optimization parameter is the arrangement of the compression springs underneath the compressor. The constraints on these arrangements were taken into account according to the physical properties of the compressor model and its outer shell. There are four different allowed symmetric arrangements that were also considered in the optimization problem, as shown in Fig. 7.

3- Experimental work

The optimization process led to a new design of springs with new arrangements. Experiments were done to support the optimization results. As it was mentioned before, the objective function was the acceleration of a specific point on the compressor with easy access.

3- 1- Laboratory equipment

3- 1- 1- Accelerometer

A Triaxial Piezo-Tronic vibration transducer was used for experimental acceleration measurements. The accelerometer model was DJB A/130/V as shown in Fig. 8 (a).

3- 1- 2- Data logger and software

To convert the output signals from the accelerometer into numerical data, B&K Lan Interface Module Type 7533 (shown in Fig. 8 (b)) was used as the data logger, and B&K PULSE-Labshop was the software used for further computations.

To attach the optimized springs to the compressor according to optimized arrangement, a new base design was required as well (Fig. 9). Both initial and optimal springs were attached to the model as shown in Fig. 10 in turn for testing and comparing the vibrational behavior of the compressor in each situation.

(a) (b)

Fig. 8. Equipment used in experimental measurements (a) DJB A/130/V Triaxial Piezo-Tronic Accelerometer (b) B&K Lan Interface Module Type 7533

(a) (b)

Fig. 9. Aluminum base for attaching springs (a) Actual made model (b) Base position under the compressor

(a) (b)

Fig. 10. Attached springs on compressor (a) Initial Model (b) Optimal model

Table 5. Initial and optimal values of optimization parameters

	d (mm)	D (mm)	N_a	ζ	Material	Arrangement No.
Initial	1.7	13.9	8	1.28	Spring Steel	4
Optimal	1.8	16.8	4	6.55	Chrome-Silicon	2

Table 6. Initial and optimal values of acceleration RMS in the mathematical model

	Initial	**Optimal**	**Reduction %**
X Acceleration RMS (m/s^2)	4.02	3.04	24.44
Y Acceleration RMS (m/s^2)	6.42	5.78	9.8
Z Acceleration RMS (m/s^2)	1.72	1.7	1.02
Total Acceleration RMS (m/s^2)	7.77	6.75	13.07

Table 7. Acceleration RMS comparison between experimental and simulation model

	Simulation	**Experimental**	**Error %**
X Acceleration RMS (m/s^2)	4.12	4.02	2.43
Y Acceleration RMS (m/s^2)	6.61	6.42	2.87
Z Acceleration RMS (m/s^2)	1.47	1.72	14
Objective Function (m/s^2)	7.92	7.76	2.02

After preparation of the setup, the far end of compression springs was fixed entirely on the ground for reducing the error caused by slip. When the compressor reached its stable vibration situation, the accelerometer data were stored. A 10 second record of the measurement signals for each case in its stable position was found to be rich enough for further calculations.

4- Results and Discussion

4- 1- Optimization results

In this study, the genetic algorithm optimization method was used to find the optimal suspension system parameters for the compressor model. The population size of 50 was chosen for the GA method. The number of generation limits was equal to variable numbers multiplied by 100, function and constraint tolerance for convergence criteria were both set to be 1e-7. Other optimization options were set to default values. The optimization program met its convergence criteria in the 136th generation. According to the results, the objective function decreased from 7.77 to 6.75 m/s^2, indicating a 13% reduction of the objective function. The initial and optimal values of parameters, initial and optimal values of Root-Mean-Square (RMS) accelerations in *X, Y, Z* directions, and total RMS (objective function) are listed in Tables 5 and 6.

4- 2- Mathematical model validation

To verify the described mathematical model, a comparison has been made between the actual model and its 6-DoF numerical simulation. The acceleration RMS response of the compressor in its stable situation for 10s was used for validation. The accelerometer was mounted at the mentioned location, and the measurement started after the compressor passed its transient behavior. The same approach was applied in the MATLAB model. The results are shown in Table 7 for comparison. It can be seen that the difference between the objective function in the experimental and simulation results is less than 3%. Therefore, the mathematical model and the following optimization can be considered reliable for further application.

4- 3- Experimental results

Our final experiments were aimed to give two comparisons

Table 9. Acceleration power comparison for initial and optimal values in the operating frequency of 50 Hz

	Initial	Optimal	Reduction %
Power in *X* direction $(m/s^2)^2$	6309.6	4639.8	26.4
Power in *Y* direction $(m/s^2)^2$	11389	9817.5	13.8
Power in *Z* direction $(m/s^2)^2$	1983.8	1419.1	4.9

between the initial and optimal suspension systems of the compressor. The first comparison is based upon the optimization objective function, which is the acceleration RMS in all three directions. The acceleration of the specified spot on the compressor is acquired from tests in its steady-state situation for 10 seconds. Individual accelerations for each direction, in addition to the overall RMS, as the objective function, are listed in Table 8.

As indicated in Tables 5 and 8, the optimization results are correlated with the experimental and mathematical models. The best improvements in each direction were sorted by *X, Z,* and then *Y.* It is noticeable that by reducing the distance between springs in *Y* direction, the compressor would rotate more freely around *X*-axis (θ), hence, the acceleration RMS in the *Y* direction would increase. However, In spite of this adverse effect on the objective function, the optimal spring design compensated the RMS increase in the *Y* direction with significant reductions along *X* and *Z*.

The second comparison was made between the initial and optimal results in the frequency domain. The power spectrum of acceleration is shown in Fig. 11. The power magnitudes of the acceleration in different directions for the operating frequency (50 Hz) are also compared in Table 9 showing the improved vibrational performance of the system.

As shown in Fig. 11, the optimal model is only more efficient than the initial model around 50 Hz, and improvements cannot be seen in other frequency ranges. The answer lies within the fact that the system has been optimized in its steady-state situation, meaning the motor has passed its quick speedup and has reached its 50 Hz rate. Considering the significant time the compressor is working on its nominal frequency of 50Hz compared to the transient short period of turning on and off, the reduction of acceleration RMS in 50 Hz should justify the optimization.

5- Conclusion

The main purpose of this study was to reduce the vibration of hermetic compressors used in conventional refrigerators. The compressor was modeled and analyzed as a 6-DoF system in MATLAB-Simulink and then in ADAMS for verification and accuracy analysis. The suspension system of the compressor was primarily considered to be optimized. The optimization was performed for five different parameters, including the main spring design variables and their arrangement under the central core of the compressor. The objective function was chosen to be the acceleration RMS for three directions of a location at the top of the compressor available for measurement. The genetic algorithm was used to determine the optimal values of the parameters. A major improvement in the vibrational behavior of the system (in both time and frequency domains) was observed at the working frequency of the system comparing the objective function for initial and optimal values.

References

[1] K. Imaichi, N. Ishii, K. Imasu, S. Muramatsu, M. Fukushima, A Vibration Source in Refrigerant Compressors, Journal of Vibration and Acoustics, 106(1) (1984) 122-128.

[2] J.M. Juran, A.B. Godfrey, Juran's Quality Handbook, McGraw Hill, 1999.

[3] H.S. Han, W.B. Jeong, M.S. Kim, S.Y. Lee, M.Y. Seo, Reduction of the refrigerant-induced noise from the evaporator-inlet pipe in a refrigerator, International Journal of Refrigeration, 33(7) (2010) 1478-1488.

[4] D. Balandin, N. Bolotnik, W. Pilkey, Optimal shock and vibration isolation, Shock and Vibration, 5(2) (1998) 73-87.

[5] T.A. Brungart, E.T. Riggs, Rotor isolation for vibration and noise reduction, Journal of vibration and acoustics, 125(3) (2003) 407-411.

[6] J. Lee, A.H. Ghasemi, C.E. Okwudire, J. Scruggs, A linear feedback control framework for optimally locating passive vibration isolators with known stiffness and damping parameters, Journal of Vibration and Acoustics, 139(1) (2017) 011006.

[7] P. Gardonio, S. Elliott, Passive and active isolation of structural vibration transmission between two plates connected by a set of mounts, Journal of Sound and Vibration, 237(3) (2000) 483-511.

[8] P. Guo, Z. Lang, Z. Peng, Analysis and design of the force and displacement transmissibility of nonlinear viscous damper based vibration isolation systems, Nonlinear Dynamics, 67(4) (2012) 2671-2687.

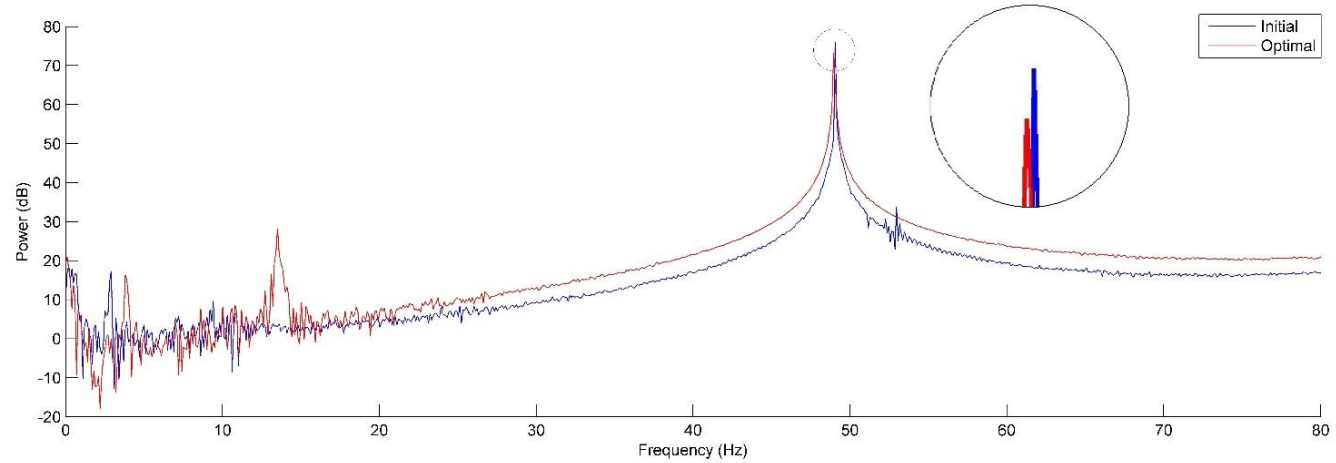

(a)

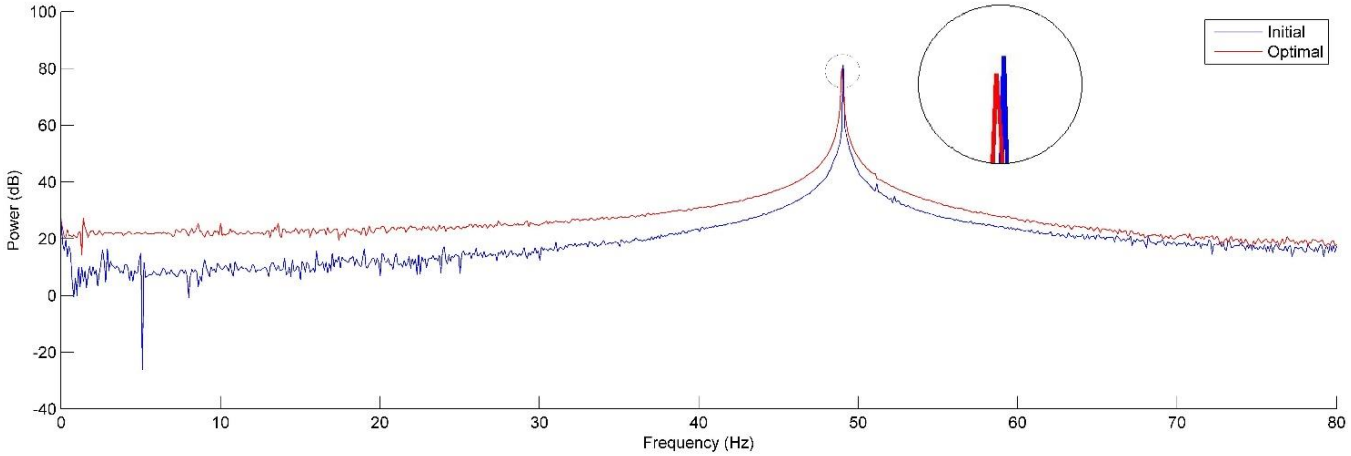

(b)

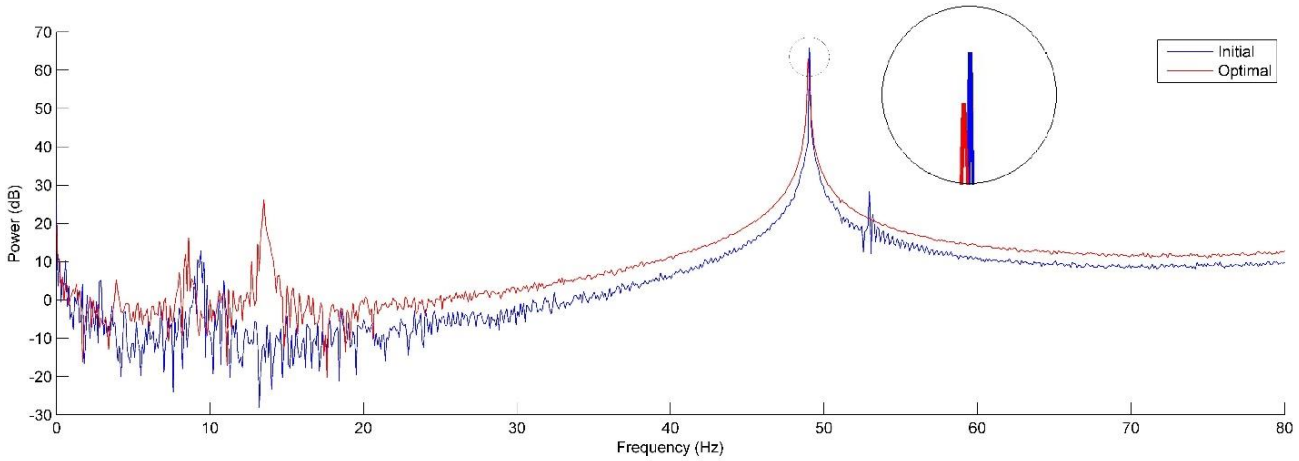

(c)

Fig. 11. Acceleration Power Spectrum for initial and optimal designs (a) X direction (b) Y direction (c) Z direction

[9] M. Zehsaz, M. Sadeghi, M. Ettefagh, F. Shams, Tractor cabin's passive suspension parameters optimization via experimental and numerical methods, Journal of Terramechanics, 48(6) (2011) 439-450.

[10] Z. Chi, Y. He, G.F. Naterer, Design optimization of vehicle suspensions with a quarter-vehicle model, Transactions of the Canadian Society for Mechanical Engineering, 32(2) (2008) 297-312.

[11] M. Mahmoodi-Kaleibar, I. Javanshir, K. Asadi, A. Afkar, A. Paykani, Optimization of suspension system of off-road vehicle for vehicle performance improvement, Journal of central south university, 20(4) (2013) 902-910.

[12] M.S. Reddy, P. Vigneshwar, M.S. Ram, D.R. Sekhar, Y.S. Harish, Comparative Optimization Study on Vehicle Suspension Parameters for Rider Comfort Based on RSM and GA, Materials Today: Proceedings, 4(2) (2017) 1794-1803.

[13] R.W. Carpick, D. Ogletree, M. Salmeron, Lateral stiffness: A new nanomechanical measurement for the determination of shear strengths with friction force microscopy, Applied Physics Letters, 70(12) (1997) 1548-1550.

[14] Z. He, Z. Jian, T. Wang, D. Li, X. Peng, Investigation on the variation of pressure in the cylinder of the refrigerator compressor based on FSI model, in: IOP Conference Series: Materials Science and Engineering, IOP Publishing, 2017, pp. 012005.

[15] G. Genta, Dynamics of rotating systems, Springer Science & Business Media, 2007.

[16] J.E. Shigley, Mechanical engineering design, (1972).

HOW TO CITE THIS ARTICLE

A. Kogani, F. A. Shirazi, M. J. Mahjoob, Suspension Design Optimization of a Hermetic Compressor for Improved Vibrational Behavior, AUT J. Mech Eng., 5(4) (2021) 497-510.

DOI: 10.22060/ajme.2021.19099.5932